AAVP displaying octreotide for ligand-directed therapeutic transgene delivery in neuroendocrine tumors of the pancreas

Tracey L. Smith[a,b], Ziqiang Yuan[c], Marina Cardó-Vila[a,b], Carmen Sanchez Claros[c], Asha Adem[c], Min-Hui Cui[d,e], Craig A. Branch[d,e], Juri G. Gelovani[f], Steven K. Libutti[c,g], Richard L. Sidman[h,1], Renata Pasqualini[a,b,1,2], and Wadih Arap[a,i,1,2]

[a]University of New Mexico Comprehensive Cancer Center, Albuquerque, NM 87131; [b]Division of Molecular Medicine, Department of Internal Medicine, University of New Mexico School of Medicine, Albuquerque, NM 87131; [c]Department of Surgery, Albert Einstein College of Medicine, Bronx, NY 10461; [d]Department of Radiology, Albert Einstein College of Medicine, Bronx, NY 10461; [e]Department of Medicine, Albert Einstein College of Medicine, Bronx, NY 10461; [f]Department of Biomedical Engineering, Wayne State University, Detroit, MI 48201; [g]Department of Genetics, Albert Einstein College of Medicine, Bronx, NY 10461; [h]Department of Neurology, Beth Israel Deaconess Medical Center, Harvard Medical School, Boston, MA 02215; and [i]Division of Hematology/Oncology, Department of Internal Medicine, University of New Mexico School of Medicine, Albuquerque, NM 87131

Contributed by Richard L. Sidman, January 4, 2016 (sent for review December 7, 2015; reviewed by Herbert Chen, James Howe, and Raphael E. Pollock)

Patients with inoperable or unresectable pancreatic neuroendocrine tumors (NETs) have limited treatment options. These rare human tumors often express somatostatin receptors (SSTRs) and thus are clinically responsive to certain relatively stable somatostatin analogs, such as octreotide. Unfortunately, however, this tumor response is generally short-lived. Here we designed a hybrid adeno-associated virus and phage (AAVP) vector displaying biologically active octreotide on the viral surface for ligand-directed delivery, cell internalization, and transduction of an apoptosis-promoting tumor necrosis factor (TNF) transgene specifically to NETs. These functional attributes of AAVP-TNF particles displaying the octreotide peptide motif (termed Oct-AAVP-TNF) were confirmed in vitro, in SSTR type 2-expressing NET cells, and in vivo using cohorts of pancreatic NET-bearing *Men1* tumor-suppressor gene KO mice, a transgenic model of functioning (i.e., insulin-secreting) tumors that genetically and clinically recapitulates the human disease. Finally, preclinical imaging and therapeutic experiments with pancreatic NET-bearing mice demonstrated that Oct-AAVP-TNF lowered tumor metabolism and insulin secretion, reduced tumor size, and improved mouse survival. Taken together, these proof-of-concept results establish Oct-AAVP-TNF as a strong therapeutic candidate for patients with NETs of the pancreas. More broadly, the demonstration that a known, short, biologically active motif can direct tumor targeting and receptor-mediated internalization of AAVP particles may streamline the potential utility of myriad other short peptide motifs and provide a blueprint for therapeutic applications in a variety of cancers and perhaps many nonmalignant diseases as well.

AAVP | neuroendocrine tumor | pancreas | phage display | preclinical study

A long-standing goal of targeted anticancer therapy is to deliver the drug solely to the tumor and eliminate toxicity to nonmalignant tissues. To this end, bacteriophage (phage)-based vectors are attractive, because ligand peptide motifs can be displayed on the pIII coat protein to allow viral binding to and internalization into target cells in vitro and in vivo (1), and the phage can be genetically modified to deliver gene products that kill tumor cells (2–7). In previous work, we combined phage and adeno-associated virus (AAV) to form a hybrid AAV/phage (termed AAVP) vector that enables superior ligand-directed delivery and cellular transduction of transgenes as a targeted platform (2). Indeed, combining the functional attributes of prokaryotic phage (i.e., robust nontoxic particles multipliable at low cost) with those of eukaryotic AAV (i.e., strong mammalian cell transduction) allows incorporation of the beneficial aspects of each into the new particle. The targeting capacities and engineered tropism for cells specifically expressing a receptor of interest permits gene expression with limited amounts of circulating AAVP after systemic administration, increasing efficacy with minimal toxicity.

The ligand-directed AAVP-based system has enabled a theranostic approach wherein a single transgene functions as a noninvasive molecular imaging reporter and therapeutic gene in preclinical models of prostate and breast cancer (2), soft-tissue sarcomas (3), and glioblastomas (4). These previous chimeric AAVP vectors were each targeted on the specific tumor type by ligand motifs identified by phage display from combinatorial peptide libraries. To date, however, no studies have shown that short peptides with known biological activity would function as a ligand displayed in viral systems used for genetic delivery, including phage, AAV, or AAVP. The use of known, biologically active peptides eliminates the need to a priori screen, identify, and validate ligand–receptor pairs with substantial time and cost savings,

Significance

There are literally thousands of biologically active, clinically relevant peptide motifs in mammalian species. Surprisingly, however, despite this abundance of potential peptide reagents for ligand-directed delivery, applications for targeted gene therapy are generally lacking. Here we used a hybrid AAV/phage (AAVP) vector for octreotide ligand-directed therapeutic gene delivery to pancreatic neuroendocrine tumors in a transgenic mouse model that faithfully recapitulates the cognate human disease. This platform is readily available for a translational clinical trial. In a broader context, this proof-of-concept work establishes a unique targeting paradigm in which existing ligand/receptors may be exploited in nature while minimizing or eliminating several rate-limiting steps of conventional phage display library selection that require cumbersome experimental discovery work.

Author contributions: T.L.S., M.C.-V., C.A.B., S.K.L., R.L.S., R.P., and W.A. designed research; T.L.S., Z.Y., M.C.-V., C.S.C., A.A., and M.-H.C. performed research; T.L.S., Z.Y., A.A., M.-H.C., and J.G.G. contributed new reagents/analytic tools; T.L.S., Z.Y., M.C.-V., C.S.C., A.A., M.-H.C., J.G.G., S.K.L., R.L.S., R.P., and W.A. analyzed data; and T.L.S., M.C.-V., S.K.L., R.L.S., R.P., and W.A. wrote the paper.

Reviewers: H.C., University of Alabama; J.H., University of Iowa Carver College of Medicine; and R.E.P., Ohio State University Wexner Medical Center.

Conflict of interest statement: J.G.G., S.K.L., R.P., and W.A. are founders of and equity holders in AAVP BioSystems. R.P. and W.A. are inventors listed on patent applications related to this work and will be entitled to standard royalties if licensing and/or commercialization occurs. The University of New Mexico Health Sciences Center currently manages these arrangements in accordance with its established institutional conflict of interest policy.

Freely available online through the PNAS open access option.

[1]To whom correspondence may be addressed. Email: richard_sidman@hms.harvard.edu, rpasqual@salud.unm.edu, or warap@salud.unm.edu.

[2]R.P. and W.A. contributed equally to this work.

This article contains supporting information online at www.pnas.org/lookup/suppl/doi:10.1073/pnas.1525709113/-/DCSupplemental.

www.pnas.org/cgi/doi/10.1073/pnas.1525709113

and reveals a minimal risk avenue for tumor attack via known ligands or receptors overexpressed specifically in tumors.

Brazeau's landmark discovery of somatostatin two decades ago (8), along with a large body of ensuing investigations (9, 10), have identified the avidity of malignant tumors overexpressing receptors for somatostatin or its analogs (SSTRs). Generally, tumors arising from neuroendocrine tissues often express at least one SSTR family member at the cell membrane level, most often SSTR type 2 (SSTR2), and thereby provide a specific path for ligand-directed targeting and molecular imaging (11). Unfortunately, the half-life of native somatostatin in the circulation is only ~2–3 min (12), which essentially eliminates its medical utility and has prompted the development of synthetic analogs (13). One such synthetic cyclic somatostatin analog, termed octreotide (single-letter residue sequence, FCFWKTCT), mimics native somatostatin but with a much longer half-life (~90 min), specific SSTR2 affinity, and potent inhibition of growth hormone and glucagon activity and insulin release (14, 15).

Human pancreatic NETs are relatively rare. The sole potentially curative intervention is surgical resection, but patients are often ineligible (i.e., with unresectable, metastatic, or inoperable tumors), leaving limited therapeutic options (16). However, given that these tumors frequently overexpress SSTR2, they often clinically respond to synthetic somatostatin analogs such as octreotide and lanreotide (16–19). Indeed, diagnostic imaging studies of SSTR targets are standard for so-called "octreotide-avid" tumors (20), and peptide-based receptor radionuclide therapy also has been used to clinical effect (21). Thus, we reasoned that octreotide-targeted cellular transduction would enable the expression of tumor necrosis factor (TNF) within the SSTR2-expressing tumor cells after systemic administration through the vulnerable tumor-associated blood vessels of pancreatic NETs without off-target vascular or parenchymal toxicity to normal organs.

TNF is an inflammatory cytokine with variable physiological and pathological functions, including antivascular and antitumor effects. Unfortunately, TNF has limited application clinically because of predictable but severe systemic toxicity, which calls for localized administration or targeted delivery (5, 6). Here we introduce an AAVP particle displaying the octreotide peptide motif to enable ligand-directed genetic TNF delivery (termed Oct-AAVP-TNF) in the preclinical context of pancreatic NETs. Our central hypothesis, evaluated in vitro, in cellulo, and in vivo, is that the motif display of a clinically active peptide, such as octreotide, in the setting of AAVP particles can functionally emulate the specific binding attributes of the native biological ligand–receptor system.

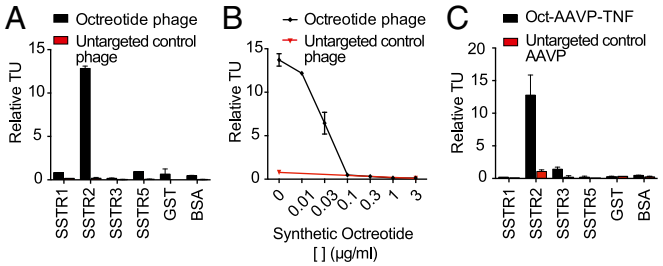

Fig. 1. Octreotide displayed in targeted viral systems binds SSTR2 specifically. (*A*) Octreotide phage or control untargeted phage binding to SSTR or control proteins adhered to a microtiter plate. Error bars indicate SD of the mean. Phage particles displaying octreotide bound preferentially to immobilized SSTR2, relative to several controls. Experiments were repeated three times in duplicates with similar results. A typical representative experiment is shown. (*B*) Octreotide phage binding was completely inhibited with increasing soluble concentrations of synthetic octreotide. Error bars indicate SD. Experiments were performed three times in duplicates with similar results. A typical representative experiment is shown. (*C*) Oct-AAVP-TNF or untargeted control AAVP-TNF binding to immobilized SSTR members or negative control proteins. Values indicated are results from a representative example of three experiments performed in duplicate. Error bars indicate SD.

Results and Discussion

Viral Particles Displaying Octreotide Specifically Bind SSTR2. Phage and AAVP displaying the octreotide peptide motif (Fig. S1) or the corresponding untargeted control constructs were designed to (*i*) evaluate the feasibility of ligand-directing viral particles via motif display of a biologically active peptide and (*ii*) determine its specific affinity for each SSTR family member. Specific receptor targeting was evaluated using a ligand binding assay against recombinant SSTR proteins tagged with GST and immobilized on a microtiter plate. Octreotide phage particles bound specifically to SSTR2, with no detectable binding above background levels for SSTR1, SSTR3, or SSTR5 (Fig. 1*A*). Untargeted control phage particles did not bind to any SSTR or control proteins.

To confirm binding specificity, we performed competitive assays of octreotide phage binding to SSTR2 after the addition of increasing concentrations of synthetic octreotide peptide. Competitive binding was inhibited in a concentration-dependent manner (Fig. 1*B*), a result indicative of ligand–receptor specificity. These experiments confirmed recapitulation of the specific SSTR2 binding activity of octreotide within the context of a phage particle.

We next generated Oct-AAVP-TNF, an AAVP construct displaying the octreotide peptide motif, to mediate targeted delivery and cellular transduction of the TNF, and reanalyzed AAVP binding specificity in vitro. Strong and specific binding was again observed for SSTR2 alone, whereas SSTR1, SSTR3, SSTR5, and control proteins (GST and BSA) exhibited minimal detectable binding over assay background (Fig. 1*C*). These results show the correct incorporation, display, and functionality of the ligand octreotide in the context of Oct-AAVP-TNF, at least in vitro.

Oct-AAVP-TNF Facilitates Cellular Transduction and Transgene Expression in NET Cells. We next analyzed Oct-AAVP-TNF targeting and activity using SSTR2-expressing NET cells. We first confirmed SSTR2 expression on the tumor cell surface using FACS with an anti-human SSTR2 antibody. These results were consistent with published reports (22). Incubating the cell suspension under ice-cold experimental conditions limited receptor internalization and allowed evaluation of SSTR2 expression on the cell surface, a biochemical requirement for ligand binding. Compared with the isogenic control antibody, NET cells exhibited markedly increased FITC expression, corresponding to an increase in anti-SSTR2 antibody binding (Fig. 2*A*).

AAVP functionality requires an initial ligand–receptor binding step, followed by cell internalization, and finally genomic integration and expression of the transgene (2, 23). Therefore, we evaluated each of these steps in human NET-derived cells. We began by quantifying Oct-AAVP-TNF binding to SSTR2 displayed on the surface of NET cells using biopanning and rapid analysis of selective interactive ligands (BRASIL) methodology (24, 25). A fivefold increase in binding of Oct-AAVP-TNF to the NET cells was observed compared with the untargeted control AAVP-TNF. This increase was completely abrogated by previous incubation with the competing soluble ligand peptide, synthetic somatostatin (SST-14) (Fig. 2*B*), demonstrating biochemical specificity for the ligand–receptor interaction.

We next evaluated peptide-mediated transmembrane internalization of Oct-AAVP-TNF particles in NET cells. Oct-AAVP-TNF, but not untargeted control AAVP-TNF, internalized into the NET cells at both 2 h and 24 h (Fig. 2*C*). A lack of immunofluorescence in the nonpermeabilized cells confirmed that rigorous washing, including multiple acid washes with a glycine buffer, was sufficient to eliminate bound AAVP from the cell surface, and also confirmed that the fluorescence seen within permeabilized NET cells was due to internalized Oct-AAVP-TNF particles alone. Fluorescence was observed in the cytoplasm of the majority of cells after administration of Oct-AAVP-TNF, with time-dependent accumulation in the experimental range studied (up to 24 h).

After confirming receptor binding and internalization, we used the NET cells to evaluate Oct-AAVP-TNF transduction via the *cis*-genomic elements of AAV (i.e., the inverted terminal repeats that mediate genetic integration and/or head-to-tail concatemerization) (2, 23). Because TNF is a secreted protein product, incubating the

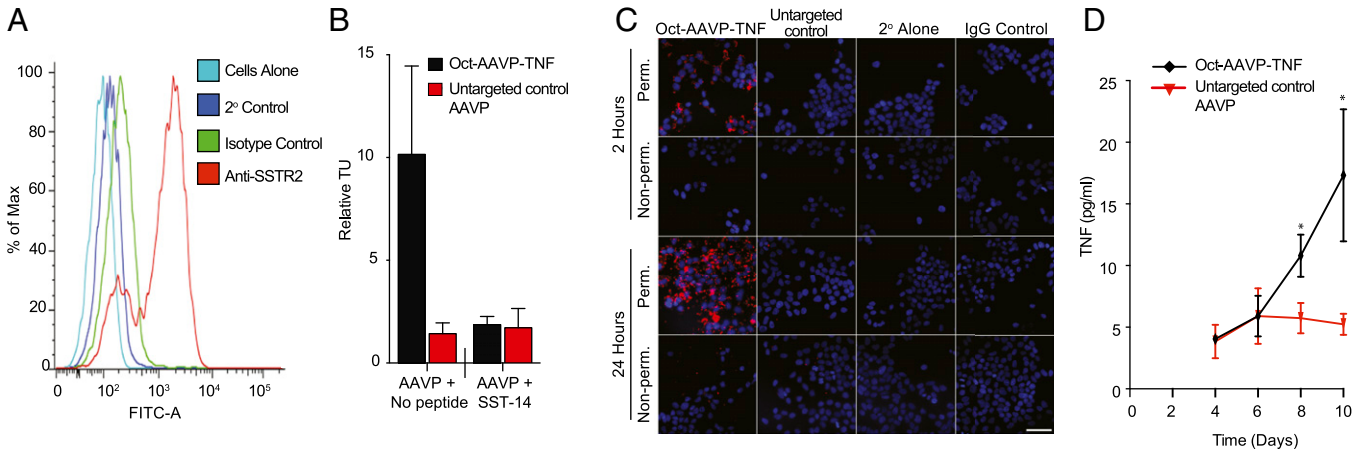

Fig. 2. Targeting and TNF generation mediated by Oct-AAVP-TNF particles binding to SSTR2-expressing human NET cells. (*A*) Human NET-derived cells were incubated with an antibody specific for human SSTR2 or isotype-matched control monoclonal antibody followed by a FITC-labeled goat anti-mouse secondary antibody. The representative histogram plot depicted shows the intensity of FITC expression determined by flow cytometry. There is a substantial (approximately sevenfold) increase in FITC expression (*x* axis) for the anti-SSTR2 population (red) compared with negative controls. (*B*) Oct-AAVP-TNF, but not untargeted control AAVP-TNF, particles bound to NET cells, and the admixture of a soluble somatostatin peptide (synthetic SST-14) abrogated AAVP binding. The experiments were repeated three times in duplicate, with similar results. A typical representative experiment is shown. Error bars indicate SD. (*C*) Oct-AAVP-TNF, but not untargeted control AAVP-TNF, was internalized into NET cells after both 2 h and 24 h of incubation. A primary antibody against bacteriophage that recognizes the phage-based portion of AAVP, followed by a Cy3-conjugated goat anti-rabbit secondary antibody, identified AAVP particles within the cells (red fluorescence) after cellular permeabilization (Perm). No phage staining was seen in cells that were not permeabilized (Non-perm). Nuclei were stained with DAPI (blue). (Scale bar: 50 μm.) (*D*) TNF expression after transduction with Oct-AAVP-TNF increased over time. Compared with untargeted control AAVP, the levels of secreted TNF found in the cell culture medium at 8 d and 10 d after transduction in the octreotide group was differentially increased. Values shown are the results of a representative experiment. Error bars indicate SD. $*P < 0.05$.

cells with either Oct-AAVP-TNF or untargeted control AAVP permitted a serial analysis of TNF expression over time. Tumor cell culture medium collected every other day for 10 d was analyzed by ELISA, which revealed a marked increase in TNF expression over time in tumor cells treated with octreotide-targeted AAVP particles, but not in untargeted controls (Fig. 2*D*). No cytotoxic effects were evident during the study, and the tumor cells remained confluent at the end of the 10-d period, confirming the results of previous studies claiming that either a supplemental or a synergistic agent must be added to the tumor cells to produce a detectable cytotoxic effect in vitro (26). It should be noted, however, that this effect is not necessarily required in vivo, in which the cytotoxic activity of TNF in activated endothelial cells of the tumor vasculature has long been recognized (27).

Oct-AAVP-TNF Particles Target Pancreatic Neuroendocrine Tumors in Vivo. After confirming specific ligand–receptor binding and targeted gene expression in vitro, we evaluated Oct-AAVP-TNF activity in vivo. Because patients diagnosed with both hereditary and sporadic pancreatic NETs often bear an *MEN1* gene mutation (28), we used a preclinical mouse model of human multiple endocrine neoplasia syndrome type 1 (MEN1). This syndrome, associated with pancreatic NETs, is characterized by insulin-secreting tumors, or insulinomas, in the islets of the endocrine pancreas (29). The tumor microenvironment of the *Men1* transgenic mouse (generated by pancreas-specific elimination of the *Men1* tumor suppressor gene) provides an opportunity to evaluate the activity of the Oct-AAVP-TNF construct in a system that closely mimics the vulnerable and fenestrated tumor

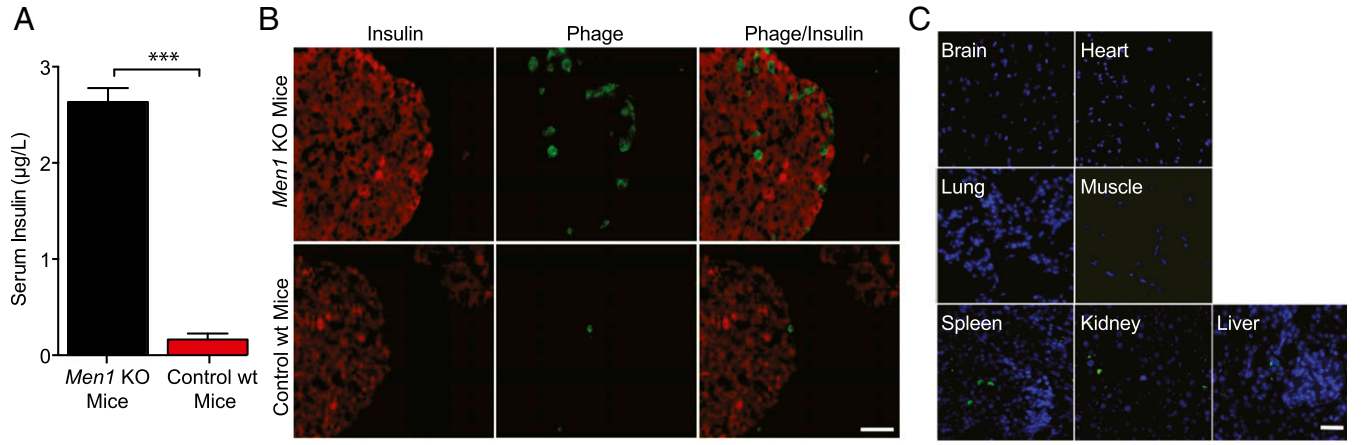

Fig. 3. Oct-AAVP-TNF localizes to functioning (insulin-secreting) NETs. (*A*) NETs of the pancreas in *Men1* transgenic mice are functional insulinomas. Compared with otherwise isogenic control mice of the same age, 12-mo-old *Men1* transgenic mice have increased levels of circulating insulin, indicating the presence of insulin-secreting tumors in the pancreas. Error bars indicate SD. $***P < 0.001$. (*B*) Oct-AAVP-TNF localized to insulinomas in *Men1* transgenic mice, but not to islets in negative control mice. On immunofluorescence analysis, evidence of AAVP homing, expressed as green fluorescence associated with anti-phage antibody binding, was observed in the insulin-secreting tumors of *Men1* transgenic mice. Anti-insulin staining (red) indicated the endocrine tissue. (Scale bar: 50 μm.) (*C*) Immunofluorescence of Oct-AAVP-TNF (green) in control organs (spleen, kidney, and liver) and negative control organs (brain, heart, lung, and muscle). (Scale bar: 50 μm.)

neovascular endothelium found pathologically in patients with MEN1 (29). Specifically, NETs of the pancreatic islets in *Men1* transgenic mice are highly vascularized, correlating with both insulinoma development and tumor progression, and tumor blood vessels show structural abnormalities that include dilation and intense tortuosity (29). Tumors in the *Men1* KO animals also express SSTR2, for targeting with octreotide (30). Given that both tumor vascularization and receptor expression are critical for AAVP activity, these data confirm the suitability of the *Men1* KO mouse model for evaluating targeted transgene delivery with Oct-AAVP-TNF particles in vivo after systemic administration.

Compared with otherwise isogenic control mice, the *Men1* transgenic mice had significantly increased serum insulin levels, indicating the presence of insulin-secreting (or "functioning") tumors (Fig. 3*A*). After the confirmation of tumor status, either octreotide or control AAVP particles were administered i.v. and allowed to circulate for 4 d, after which the target tissues were recovered and analyzed initially for AAVP homing in vivo. Oct-AAVP-TNF was found to localize specifically in the insulinomas of the *Men1* KO mice, but was not found in the islets of control animals (Fig. 3*B*). Evaluation of normal organs and tissues recovered from the *Men1* KO mice revealed anti-phage fluorescence within the spleen, liver, and kidney (Fig. 3*C*). AAVP particles are commonly identified in organs of the mononuclear phagocyte system, or reticuloendothelial system (RES), including the spleen, liver, and kidneys, and represents the long-recognized transient, nonspecific retention of particle processing, degradation, and excretion in vivo (6, 31, 32).

TNF Expression Originates Solely from Pancreatic NETs. To evaluate the transduction capacity of Oct-AAVP-TNF, we quantified transgene expression in the recovered tissue at both protein and RNA levels. ELISA analysis of human TNF protein expression in the pancreas (including any tumors) and control organs identified TNF in the pancreas only in the *Men1* transgenic mice and not in the control mice, with no TNF detected in the control organs (including the RES organs) from either experimental group (Fig. 4*A*). These findings further support the likelihood that the AAVP particles in those organs detected by immunofluorescence (Fig. 3*C*) represent particle processing rather than nonspecific targeting.

Laser capture microdissection (LCM) enabled the evaluation of NET and exocrine tissue separately to determine the origin of the pancreatic TNF expression (33) (Fig. 4*B*). Using real-time quantitative RT-PCR, we first measured human TNF RNA levels and confirmed the ELISA results, with TNF expression evident in appreciable amounts only in the pancreas, and not in control organs, of the *Men1* mice following Oct-AAVP-TNF administration. TNF levels in *Men1* mice treated with untargeted control AAVP-TNF did not exceed the barely detectable background levels. Strikingly, separate measurement of normal pancreatic exocrine tissue and endocrine pancreatic tumors by LCM revealed that the pancreatic TNF expression originated solely from the insulin-secreting tumors (Fig. 4*C*). In contrast, LCM of the parathyroid gland from the thyroid confirmed the lack of transduction of nontumoral endocrine glands and thus the targeting specificity of Oct-AAVP-TNF.

Preclinical in Vivo Studies Demonstrate Antitumor Activity of Oct-AAVP-TNF. Given that Oct-AAVP-TNF localized to insulinomas in the *Men1* transgenic mice and TNF was subsequently expressed in the tumors, we concluded that the Oct-AAVP-TNF is suitable for targeted gene delivery to pancreatic NETs, and thus initiated intermediate- and long-term therapeutic studies in a preclinical setting. An intermediate duration (28-d) study served to evaluate the tumor response to a single i.v. administration of Oct-AAVP-TNF or untargeted control AAVP-TNF in the *Men1* mouse model. Tumors were imaged before treatment (baseline) and again at 28 d after AAVP treatment to evaluate the therapeutic effect of a single dose on the NETs in these animals. Magnetic resonance imaging (MRI) revealed a clear decrease in tumor size in the Oct-AAVP-TNF treatment group at 28 d after the single dose (Fig. 5*A*). All five tumors in the Oct-AAVP-TNF treatment cohort decreased significantly in size (by $73 \pm 21\%$; $P < 0.01$), whereas all three tumors in the untargeted control cohort more than doubled in size, by as much as $116 \pm 29\%$ ($P < 0.05$) (Fig. 5*B*).

It is possible to differentiate malignant pancreatic tumors from benign tumors by estimating total choline (tCho) levels via magnetic resonance spectroscopy (MRS) (34). Therefore, we analyzed the effect on tCho levels before and after treatment with Oct-AAVP-TNF. At 4 wk after treatment, the in vivo ^{1}H-MRS–estimated tCho levels decreased from an average level of

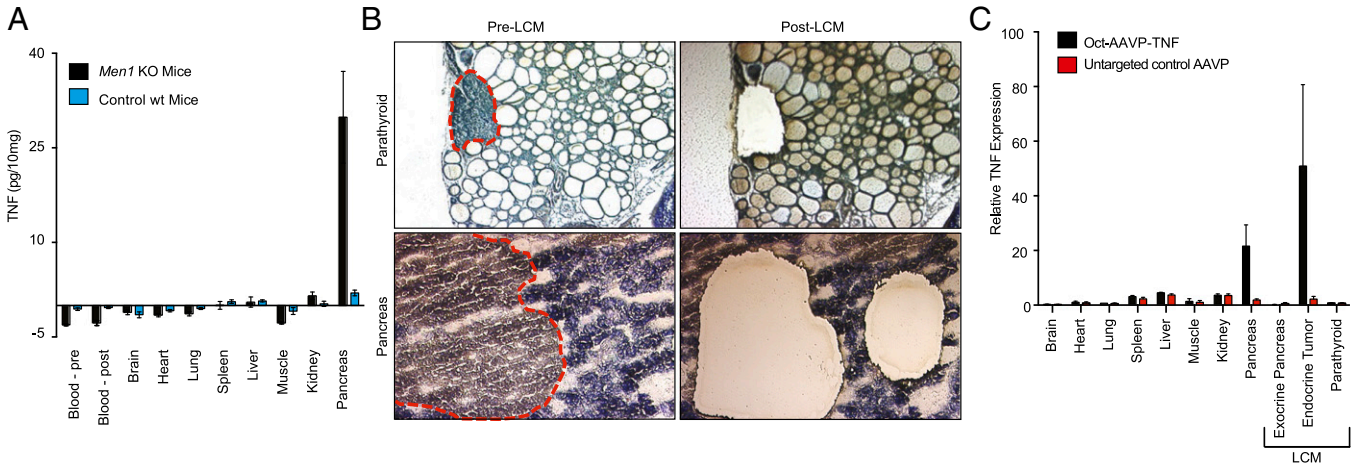

Fig. 4. TNF originates solely from pancreatic NETs after Oct-AAVP-TNF treatment. (*A*) TNF expression, measured by ELISA, was much higher in the pancreas of *Men1* transgenic mice compared with the pancreas of control mice receiving octreotide-targeted AAVP. No TNF expression was observed in the control organs or blood collected before and after administration of Oct-AAVP-TNF. Values were determined from the analysis of duplicate samples of blood or tissue from each of the three animals per group. Error bars indicate SD. (*B*) Representative experiment of a section of parathyroid and pancreas before (*Left*) and after (*Right*) LCM used to isolate endocrine and exocrine tissue. (*C*) Quantitative real-time RT-PCR revealed increased TNF expression in the pancreas of animals treated with Oct-AAVP-TNF compared with control organs or tissues from animals receiving untargeted control AAVP. Independent assessment of pancreatic NETs and exocrine tissue after isolation and extraction by LCM indicated that TNF expression in mice treated with Oct-AAVP-TNF originated solely from the pancreatic NETs, with no appreciable TNF expression found in the exocrine tissue. Values were determined from the analysis of duplicate samples of each tissue from each of three individual *Men1* transgenic mice and standardization with an 18S rRNA internal control. Error bars indicate SD.

21 ± 22 to 9 ± 12 (all $\times 10^4$). All mice showed decreases in tCho levels after a single treatment with Oct-AAVP-TNF particles, whereas mice in the control group showed increases in tCho levels after 28 d (Fig. 5*C*). These results are particularly encouraging, considering that we previously correlated tCho levels with surrogate development of NETs, identification of malignant lesions, and response to therapy, with the tCho levels reflecting the well-recognized high levels of tumor metabolism (34).

Finally, in a long-term therapy study, cohorts of mice injected weekly over 2 mo with Oct-AAVP-TNF particles showed a strong and sustained decrease in serum insulin over the experimental timeframe compared with animals injected with untargeted control AAVP (Fig. 5*D*). Of note, because many of the challenges for patients with pancreatic NETs (particularly those with functioning tumors) arise from hormonal hypersecretion and tumor-associated metabolic burden (35), meaningful results that show an unequivocal reduction in both metabolic activity and/or secreted insulin after treatment are clinically relevant. This experimental design mimics the experimental preclinical dosing schedule reported by our group in large animals (dogs) with native malignant tumors (5), and confirms the efficacy of repetitive AAVP administration serially over time, likely owing to additional cellular transduction after each administration and a bystander effect observed with AAVP activity related to the exposure of neighboring cells to cytotoxic TNF generated by transduced cells (36).

Transduction efficiency is difficult to quantify in vivo, particularly without an imaging component in the vector system (7). Evaluating agents to increase transduction efficiency (37) or direct TNF-mediated signaling cascades toward induction of apoptosis (7) could be useful for maximizing the efficacy of AAVP-based therapy and overcoming these limitations related to viral gene delivery. Importantly, mice treated with Oct-AAVP-TNF also showed a significant increase in overall survival compared with mice treated with untargeted control AAVP (Fig. 5*E*). Taken together, these preclinical results provide justification for further studies to optimize dose and determine the most efficacious dosing schedule and strongly support Oct-AAVP-TNF as a promising antitumor candidate for clinical translation in humans with pancreatic NETs.

Conclusion

We have demonstrated that a biologically active peptide can be successfully used as a displayed ligand in either phage or AAVP particles. We chose the octreotide peptide motif as a soluble cyclic octapeptide synthesized with natural residues (to enable incorporation of the encoding single-stranded DNA into viral particles), favorable pharmacologic attributes, and a very well established profile and track record for targeted drug delivery to NETs of the pancreas. The framework used here is suitable for a myriad of other known, short, biologically active peptide motifs that could enable in vivo tumor homing and/or receptor binding internalization of targeted AAVP particles to obviate or even eliminate several of the logistic requirements for combinatorial selection and validation from phage libraries in vivo.

This tumor cell-specific ligand–receptor approach could address currently unmet needs (38–40) in patients with unresectable, inoperable, or metastatic pancreatic NETs. Indeed, we have shown that Oct-AAVP-TNF reduced tumor size, metabolic activity, and hormone secretion, and also increased survival in the *Men1* transgenic mouse model, which faithfully recapitulates human disease with respect to both progression and response to therapy (29, 30). These results mimic the goals for patients with pancreatic NETs, warranting further translational investigation with Oct-AAVP-TNF. This targeted gene delivery technology could proceed rapidly for NET patients with octreotide-avid pancreatic tumors identified with imaging studies using somatostatin receptor scintigraphy (SRS) for delivery of therapeutic agents (41). Given that in cancer medicine, physicians often use somatostatin analogs to treat pancreatic NETs following imaging studies with radiolabeled octreotide to localize tumors (42), it can be postulated that tumor homing and localization of the octreotide-targeted AAVP particles—produced under good

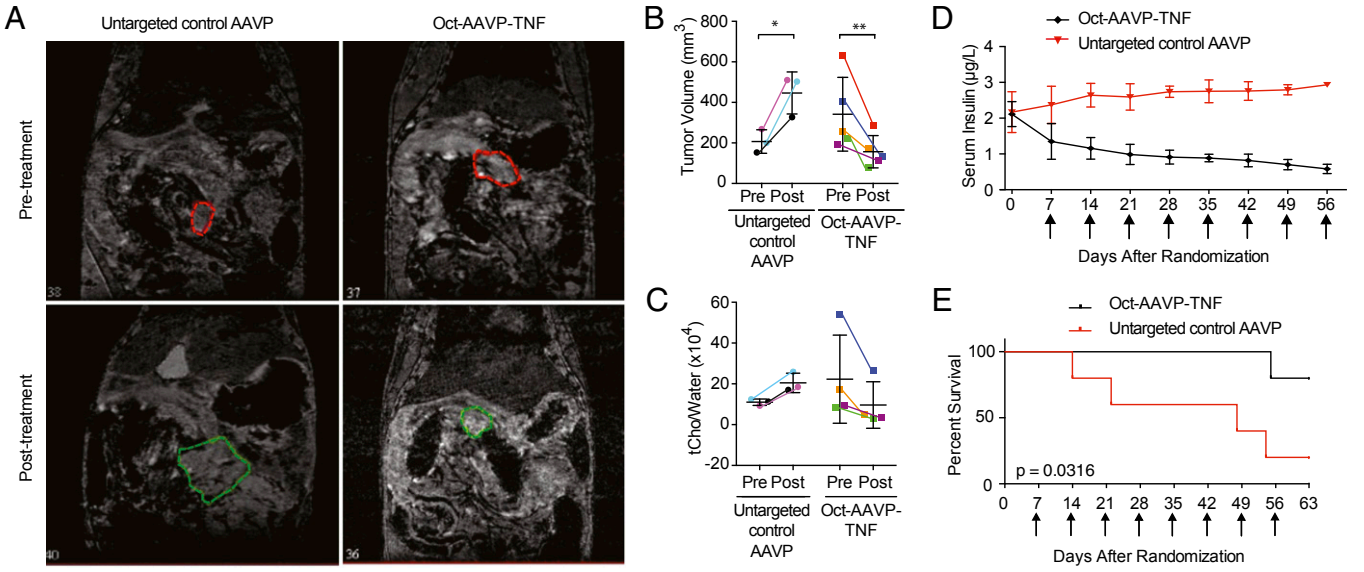

Fig. 5. Oct-AAVP-TNF treatment induces an antitumor response. (*A*–*C*) Tumor response to a single administration of Oct-AAVP-TNF. (*A*) *Men1* KO mice were imaged initially at baseline and again at 4 wk after treatment with a single dose of either targeted Oct-AAVP-TNF or untargeted control AAVP-TNF. Tumors are indicated by colored lines. (*B*) Tumor volume for treatment cohorts are described in the scatterplot, with mean and SD values indicated. Individual animals are indicated by different-colored dots. The Oct-AAVP-TNF treatment cohort showed a significant decrease in tumor size compared with baseline. In contrast, the control cohort demonstrated a significant increase in tumor size compared with baseline. $*P < 0.05$; $**P < 0.01$. (*C*) In vivo ^{1}H-MRS estimated tCho levels (tCho/water) in the pancreas of *Men1* KO mice before and after treatment with Oct-AAVP-TNF. At 4 wk posttreatment, ^{1}H-MRS estimated tCho levels (tCho/water) were decreased for all animals in the octreotide treatment group. In *B* and *C*, values are reported as mean ± SD. Colored markers indicate individual mice. (*D* and *E*) Serial response to multiple AAVP doses over time. Arrows indicate the days of AAVP administration. (*D*) Insulin levels over time, measured weekly, were decreased in the *Men1* mice treated with weekly doses of Oct-AAVP-TNF compared with *Men1* mice treated with untargeted control AAVP-TNF. (*E*) Increased survival was observed in the Oct-AAVP-TNF treatment cohort compared with mice treated with untargeted control AAVP-TNF.

manufacturing practice conditions—to the same cells and tumor sites revealed after routine SRS imaging in patients presumably would be feasible. Finally, the experimental framework used here is suitable for any biologically active motifs that could enable in vivo tumor homing and/or receptor binding internalization of targeted AAVP particles to obviate or even eliminate several of the logistic requirements for combinatorial ligand selection and validation from peptide libraries in vivo.

Materials and Methods

Design, Generation, and Production of Viral Particles. Viral constructs (filamentous phage and AAVP) displaying the octreotide peptide motif were generated according to standard protocols for viral particle production modified for incorporation of DNA sequences encoding display peptides (24, 43) (Fig. S1). Oct-AAVP-TNF constructs were designed and generated from established experimental protocols (23, 24). For production of the original viral stock particles and subsequent preparations, an individual host bacterial colony containing the correct insert sequence was amplified as described previously (23). Octreotide constructs were titrated in parallel with the corresponding negative control constructs by bacterial infection with K91Kan *Escherichia coli* to determine the number of transducing units (TU) as described previously (24).

Animal Care. Cohorts of male and female 12-mo-old (25–30 g) Pdx1-Cre; Men1f/f transgenic mice (FVB.129 background) and control mice were used in the animal experiments (29). All mice were maintained in accordance with appropriate institutional standards, and all experiments were conducted in compliance with the guidelines of the Institutional Animal Care and Use Committee of the Albert Einstein College of Medicine.

Statistical Analysis. Statistical analyses were performed with Microsoft Excel or GraphPad Prism version 6.0e. Error bars indicate the SD of the mean. Significance was determined between indicated groups using the Student *t* test. A P value <0.05 was considered statistically significant. $*P < 0.05$; $**P < 0.01$; $***P < 0.001$.

Additional methods are detailed in *SI Materials and Methods*. Receptor binding and competitive inhibition assays were performed as described previously (25, 44). Cell culture and functional assays in NET cells were completed. Flow cytometry was used to demonstrate SSTR2 expression. AAVP activity in NET cells was evaluated using cell binding (24, 25), internalization (45), and transgene expression (6, 23) assays. *Men1* transgenic mice (29) were studied for AAVP homing, human TNF expression (5–7), antitumor activity (34), and survival after treatment.

ACKNOWLEDGMENTS. This work was supported in part by the 2012 Caring for Carcinoid Foundation–American Association for Cancer Research (AACR) Grant for Carcinoid Tumor and Pancreatic Neuroendocrine Tumor Research (Grant 12-60-33-PASQ to R.P., W.A., and S.K.L.) and an award from the Gillson Longenbaugh Foundation (to W.A. and R.P.).

1. Smith GP (1985) Filamentous fusion phage: Novel expression vectors that display cloned antigens on the virion surface. *Science* 228(4705):1315–1317.
2. Hajitou A, et al. (2006) A hybrid vector for ligand-directed tumor targeting and molecular imaging. *Cell* 125(2):385–398.
3. Hajitou A, et al. (2008) A preclinical model for predicting drug response in soft-tissue sarcoma with targeted AAVP molecular imaging. *Proc Natl Acad Sci USA* 105(11):4471–4476.
4. Staquicini FI, et al. (2011) Systemic combinatorial peptide selection yields a non-canonical iron-mimicry mechanism for targeting tumors in a mouse model of human glioblastoma. *J Clin Invest* 121(1):161–173.
5. Paoloni MC, et al. (2009) Launching a novel preclinical infrastructure: Comparative Oncology Trials Consortium-directed therapeutic targeting of TNFalpha to cancer vasculature. *PLoS One* 4(3):e4972.
6. Tandle A, et al. (2009) Tumor vasculature-targeted delivery of tumor necrosis factor-alpha. *Cancer* 115(1):128–139.
7. Yuan Z, et al. (2013) Blockade of inhibitors of apoptosis (IAPs) in combination with tumor-targeted delivery of tumor necrosis factor-α leads to synergistic antitumor activity. *Cancer Gene Ther* 20(1):46–56.
8. Brazeau P, et al. (1973) Hypothalamic polypeptide that inhibits the secretion of immunoreactive pituitary growth hormone. *Science* 179(4068):77–79.
9. Patel YC (1999) Somatostatin and its receptor family. *Front Neuroendocrinol* 20(3):157–198.
10. Lamberts SW, Krenning EP, Reubi JC (1991) The role of somatostatin and its analogs in the diagnosis and treatment of tumors. *Endocr Rev* 12(4):450–482.
11. Kvols LK, et al. (1992) The presence of somatostatin receptors in malignant neuroendocrine tumor tissue predicts responsiveness to octreotide. *Yale J Biol Med* 65(5): 505–518; discussion 531–536.
12. Sheppard M, et al. (1979) Metabolic clearance and plasma half-disappearance time of exogenous somatostatin in man. *J Clin Endocrinol Metab* 48(1):50–53.
13. Oberg K, et al. (2004) Consensus report on the use of somatostatin analogs for the management of neuroendocrine tumors of the gastroenteropancreatic system. *Ann Oncol* 15(6):966–973.
14. Lamberts SW, van der Lely AJ, de Herder WW, Hofland LJ (1996) Octreotide. *N Engl J Med* 334(4):246–254.
15. Bauer W, et al. (1982) SMS 201-995: A very potent and selective octapeptide analogue of somatostatin with prolonged action. *Life Sci* 31(11):1133–1140.
16. Kunz PL (2015) Carcinoid and neuroendocrine tumors: Building on success. *J Clin Oncol* 33(16):1855–1863.
17. Kunz PL, et al.; North American Neuroendocrine Tumor Society (2013) Consensus guidelines for the management and treatment of neuroendocrine tumors. *Pancreas* 42(4):557–577.
18. Delaunoit T, Neczyporenko F, Rubin J, Erlichman C, Hobday TJ (2008) Medical management of pancreatic neuroendocrine tumors. *Am J Gastroenterol* 103(2):475–483, quiz 484.
19. Kulke MH, et al.; North American Neuroendocrine Tumor Society (NANETS) (2010) NANETS treatment guidelines: Well-differentiated neuroendocrine tumors of the stomach and pancreas. *Pancreas* 39(6):735–752.
20. Squires MH, 3rd, et al. (2015) Octreoscan versus FDG-PET for neuroendocrine tumor staging: A biological approach. *Ann Surg Oncol* 22(7):2295–2301.
21. van der Zwan WA, et al. (2015) GEPNETs update: Radionuclide therapy in neuroendocrine tumors. *Eur J Endocrinol* 172(1):R1–R8.
22. Ono K, et al. (2007) Somatostatin receptor subtypes in human non-functioning neuroendocrine tumors and effects of somatostatin analogue SOM230 on cell proliferation in cell line NCI-H727. *Anticancer Res* 27(4B):2231–2239.
23. Hajitou A, et al. (2007) Design and construction of targeted AAVP vectors for mammalian cell transduction. *Nat Protoc* 2(3):523–531.
24. Christianson DR, Ozawa MG, Pasqualini R, Arap W (2007) Techniques to decipher molecular diversity by phage display. *Methods Mol Biol* 357:385–406.
25. Giordano RJ, Cardó-Vila M, Lahdenranta J, Pasqualini R, Arap W (2001) Biopanning and rapid analysis of selective interactive ligands. *Nat Med* 7(11):1249–1253.
26. Ruggiero V, Latham K, Baglioni C (1987) Cytostatic and cytotoxic activity of tumor necrosis factor on human cancer cells. *J Immunol* 138(8):2711–2717.
27. Watanabe N, et al. (1988) Toxic effect of tumor necrosis factor on tumor vasculature in mice. *Cancer Res* 48(8):2179–2183.
28. Jiao Y, et al. (2011) DAXX/ATRX, MEN1, and mTOR pathway genes are frequently altered in pancreatic neuroendocrine tumors. *Science* 331(6021):1199–1203.
29. Shen HC, et al. (2009) Recapitulation of pancreatic neuroendocrine tumors in human multiple endocrine neoplasia type I syndrome via Pdx1-directed inactivation of Men1. *Cancer Res* 69(5):1858–1866.
30. Quinn TJ, et al. (2012) Pasireotide (SOM230) is effective for the treatment of pancreatic neuroendocrine tumors (PNETs) in a multiple endocrine neoplasia type 1 (MEN1) conditional knockout mouse model. *Surgery* 152(6):1068–1077.
31. Pasqualini R, Koivunen E, Ruoslahti E (1997) Alpha v integrins as receptors for tumor targeting by circulating ligands. *Nat Biotechnol* 15(6):542–546.
32. Pasqualini R, Ruoslahti E (1996) Organ targeting in vivo using phage display peptide libraries. *Nature* 380(6572):364–366.
33. Yao VJ, et al. (2005) Targeting pancreatic islets with phage display assisted by laser pressure catapult microdissection. *Am J Pathol* 166(2):625–636.
34. Cui MH, et al. (2015) In vivo proton MR spectroscopy of pancreatic neuroendocrine tumors in a multiple endocrine neoplasia type 1 conditional knockout mouse model. *Magn Reson Med* 74(5):1221–1226.
35. Modlin IM, et al. (2008) Gastroenteropancreatic neuroendocrine tumours. *Lancet Oncol* 9(1):61–72.
36. Trepel M, et al. (2009) A heterotypic bystander effect for tumor cell killing after adeno-associated virus/phage-mediated, vascular-targeted suicide gene transfer. *Mol Cancer Ther* 8(8):2383–2391.
37. Stoneham CA, Hollinshead M, Hajitou A (2012) Clathrin-mediated endocytosis and subsequent endo-lysosomal trafficking of adeno-associated virus/phage. *J Biol Chem* 287(43):35849–35859.
38. Baldelli R, et al. (2014) Somatostatin analogs therapy in gastroenteropancreatic neuroendocrine tumors: Current aspects and new perspectives. *Front Endocrinol (Lausanne)* 5:7.
39. Kulke MH (2015) Sequencing and combining systemic therapies for pancreatic neuroendocrine tumors. *J Clin Oncol* 33(14):1534–1538.
40. Cives M, Strosberg J (2015) The expanding role of somatostatin analogs in gastroenteropancreatic and lung neuroendocrine tumors. *Drugs* 75(8):847–858.
41. Krenning EP, et al. (1993) Somatostatin receptor scintigraphy with [111In-DTPA-D-Phe1]- and [123I-Tyr3]-octreotide: The Rotterdam experience with more than 1000 patients. *Eur J Nucl Med* 20(8):716–731.
42. Delaunoit T, Rubin J, Neczyporenko F, Erlichman C, Hobday TJ (2005) Somatostatin analogues in the treatment of gastroenteropancreatic neuroendocrine tumors. *Mayo Clin Proc* 80(4):502–506.
43. Smith GP, Scott JK (1993) Libraries of peptides and proteins displayed on filamentous phage. *Methods Enzymol* 217:228–257.
44. Cardó-Vila M, Arap W, Pasqualini R (2003) Alpha v beta 5 integrin-dependent programmed cell death triggered by a peptide mimic of annexin V. *Mol Cell* 11(5):1151–1162.
45. Arap MA, et al. (2004) Cell surface expression of the stress response chaperone GRP78 enables tumor targeting by circulating ligands. *Cancer Cell* 6(3):275–284.